Random Flow Generation Technique for Large Eddy Simulations and Particle-Dynamics Modeling

A. Smirnov, S.Shi, I. Celik
West Virginia University
Department of Mechanical and Aerospace Engineering
Morgantown, WV26506-6106
Email: andrei@smirnov.mae.wvu.edu

Abstract

A random flow generation (RFG) technique is presented, which can be used for initial/inlet boundary generation in LES (Large-Eddy-Simulations) or particle tracking in LES/RANS (Reynolds-Averaged Navier-Stokes) computations of turbulent flows. The technique is based on previous methods of synthesizing divergence-free vector fields from a sample of Fourier harmonics and allows to generate non-homogeneous anisotropic flow field representing turbulent velocity fluctuations. It was validated on the cases of boundary layer and flat plate flows. Applications of the technique to LES and particle tracking are considered.

Nomenclature

DNS	Direct Numerical Simulation
LES	Large Eddy Simulation
NS	Navier Stokes
RANS	Reynolds Averaged Navier Stokes equation
RFG	Random Flow Generation
PD	Particle Dynamics
l	Length scale of turbulence
τ	Time scale of turbulence

1 Introduction

In a Reynolds Averaged Navier-Stokes (RANS) turbulence modeling approach information about turbulent fluctuations is contained in the time averaged Reynolds stresses

of the form $\overline{u_i u_j}$. These are obtained as an outcome of a turbulence model that links Reynolds Stresses to mean flow quantities (e.g. k-ϵ model), or solves modeled transport equations for each Reynolds stress component (e.g. Reynolds Stress models). However, this is not the case when the large eddy simulation (LES) methodology is employed since the goal here is to explicitly resolve the turbulent fluctuations. In LES the inlet conditions can not be derived directly from experimental results, because of the unsteady and pseudo-random nature of the flow being resolved, unless, off course, the turbulent intensity is zero at the inlet, which is rarely the case. This problem becomes more important for spatially developing turbulent flows where for example the boundary or shear layer thickness changes rapidly. In such cases periodic boundary conditions can not be specified like in the case of a fully developed channel flow (Ravikanth and Pletcher, 2000; Akselvoll and Moin, 1995). A similar situation exists when prescribing the initial conditions over the whole calculation domain. This can be of importance when the turbulent flow is not steady in the mean (i.e. non-stationary turbulence) and the transients of the flow are to be resolved. Even for stationary turbulent flows, if realistic initial conditions are not prescribed, the establishment of a fully developed turbulence takes unreasonably long execution time. For these reasons it is necessary to initialize the flow-field with some form of perturbation to provide the initial turbulent conditions. It is important that the perturbation be spatially correlated, as is the case with the real flow. For external flow problems the turbulent flow field can be initiated simply by appropriately perturbing the inlet flow-field. In this case an accurate representation of temporal correlations of the flow-field can be important. The inlet perturbation propagates throughout the domain and helps trigger the turbulence that is to be captured. Many applications of LES begin with initializing the flow field to that of a previously obtained RANS solution. A higher resolution grid is then used with an appropriate sub-grid-scale model. The Reynolds stress terms provided by the RANS solution can be used to construct spatially and temporally correlated perturbed inlet and initial conditions. In principle it is possible to predict turbulence via LES technique by starting from a quiescent flow or with the mean flow obtained from RANS. Unfortunately, it takes a very long time for a turbulent flow to develop spatially and temporally. This is especially true in the case of decaying turbulence in the absence of strong turbulence generating factors like walls. A reasonably accurate approach to this problem is used in modeling of boundary layer turbulence (Lund, 1998). It consists in applying a separate flow solver with periodic boundary conditions to construct the inlet conditions for the LES/DNS solver. It provides well-formed inflow conditions consistent with the solution of the Navier-Stocks equation, which makes it particularly suitable for DNS. However, its implementation may not be straightforward for the problems without well defined fully developed boundary/shear layers. For some engineering problems it may also be too expensive in the usage of computer resources and programming effort.

To remedy this problem the inlet and initial conditions are often viewed as consisting of a mean component and a randomly fluctuating component with the appropriate statistics. Most of the work done in this direction is based on simplified variants of a spectral method, in which Fourier harmonics are generated with the appropriate statis-

tics and assembled into a random flow-field. Realistic turbulence spectra can be realized in this way. In the work of Lee et al. (1992) for example, a very good representation of turbulence spectra was achieved by using Fourier harmonics with a random phase shift. This is a rather efficient method to generate the inflow turbulence with pre-defined characteristics. However, it does not satisfy the continuity of the flow-field, which may be important in diminishing the non-physical transition region between the inlet flow-field and the solution provided by the Navier-Stokes solver inside the computational domain.

A considerable amount of work in random flow generation has been performed in the area of particle dispersion modeling using the RANS approach (Zhou and Leschziner, 1991; Zhou and Leschziner, 1996; Li et al., 1994). RANS modeling produces smooth flow fields, which do not accurately disperse particles that are embedded in the flow. To correct this turbulent Reynolds stresses are used to generate temporally and spatially correlated fluctuations, such that the resultant instantaneous velocity can be superimposed on the particles to induce a realistic dispersion. A number of approaches found in the literature (Li et al., 1994; Bechara et al., 1994; Fung et al., 1992) are based on a variant of spectral method of generating an isotropic continuous flow-field proposed earlier by Kraichnan (1970). However, this flow-field does not satisfy the requirement of spatial inhomogeneity and anisotropy of turbulent shear stresses, which may be important in realistic flows. The method of Zhou and Leschziner (1991) complies with the latter requirement, but the resultant flow field does not satisfy the continuity condition and is spatially uncorrelated. For homogeneous isotropic turbulence, the initial conditions can also be constructed as described by Ferziger (1983). The approach is based on a vector curl operation and forward/backward Fourier transforms, which require a considerable computational effort. The extension of this method to anisotropic inhomogeneous flows is not trivial. At least one study presents a successful application of Kraichnan's method to anisotropic flows (Maxey, 1987). The technique is based on filtering and scaling operations applied to the generated isotropic flow-field to filter only the vectors with the prescribed correlations. Again, the filtering operation may be expensive computationally. The method presented in this paper is different in that it is based only on scaling and simple coordinate transformation operations, which are efficient and fast.

It is the objective of this study to formulate a relatively simple random flow generation (RFG) algorithm, which can be used to prescribe inlet conditions as well as initial conditions for spatially developing inhomogeneous, anisotropic turbulent flows. In principle the same procedure can also be used for initializing direct numerical simulations, but the focus of our study is on LES, and particle tracking applications. The method takes advantage of the previous studies in the area of particle dispersion (Li et al., 1994; Maxey, 1987). The RFG procedure is developed on the basis of the work of Kraichnan (1970), and can be used as an efficient random flow-field generator in LES and in particle tracking (Shi et al., 2000; Smirnov et al., 2000). The technique was validated on the cases of boundary-layer and flat-plate shear layer flows and is further illustrated on the example of bubbly ship-wake flow as one of the most challenging

cases for LES and particle dynamics applications. Performing LES of ship wakes is particularly difficult given the fact that the whole ship must be modeled to capture a relatively thin 3D-boundary layer, preferably including the viscous sub-layer. The boundary layer is the source of the flow dynamics that sets the initial conditions for the wake. A simulation that includes the whole ship and the wake would require prohibitively large computational resources. It is proposed in this study that the needed computational resources could be substantially reduced if the appropriate time-dependent inlet conditions could be constructed at the beginning of the wake, thus avoiding the need to model the entire ship.

2 Methodology

To generate a realistic flow field we propose a modified version of Kraichnan's technique (Kraichnan, 1970). The procedure we call RFG (Random Flow Generation) combines the advantages of the approaches mentioned above and is also computationally efficient. It involves scaling and orthogonal transformation operations applied to a continuous flow-field generated as a superposition of harmonic functions. The procedure consists of the following steps.

1. Given an anisotropic velocity correlation tensor

$$r_{ij} \equiv \overline{\tilde{u}_i \tilde{u}_j} \tag{1}$$

of a turbulent flow field $\{\tilde{u}_i(x_j,t)\}_{i,j=1..3}$, find an orthogonal transformation tensor a_{ij} that would diagonalize r_{ij} [1]

$$a_{mi}a_{nj}r_{ij} = \delta_{mn}c^2_{(n)} \tag{2}$$

$$a_{ik}a_{kj} = \delta_{ij} \tag{3}$$

As a result of this step both a_{ij} and c_n become known functions of space. Coefficients $c_n = \{c_1, c_2, c_3\}$ play the role of turbulent fluctuating velocities (u', v', w') in the new coordinate system produced by transformation tensor a_{ij}.

2. Generate a transient flow-field in a three-dimensional domain $\{v_i(x_j,t)\}_{i,j=1..3}$ using the modified method of Kraichnan (Kraichnan, 1970)

$$v_i(\vec{x},t) = \sqrt{\frac{2}{N}} \sum_{n=1}^{N} [p_i^n \cos(\tilde{k}_j^n \, \tilde{x}_j + \omega_n \tilde{t})$$

[1] $f_{,i} \equiv \frac{\partial f}{\partial x_i}$. Repeated sub-indexes imply summation, parentheses around indexes preclude summation.

$$+ q_i^n \sin(\tilde{k}_j^n \tilde{x}_j + \omega_n \tilde{t})] \tag{4}$$

$$\tilde{x}_j = \frac{x_j}{l},\ \tilde{t} = \frac{t}{\tau},\ c = \frac{l}{\tau},\ \tilde{k}_j^n = k_j^n \frac{c}{c_{(j)}} \tag{5}$$

$$p_i^n = \varepsilon_{ijm} \zeta_j^n k_m^n,\ q_i^n = \varepsilon_{ijm} \xi_j^n k_m^n \tag{6}$$

$$\zeta_i^n,\ \xi_i^n,\ \omega_n \in N(0,1),\ k_i^n \in N(0,1/2)$$

where l, τ are the length and time-scales of turbulence, ε_{ijk} is the permutation tensor used in vector product operation (Spain, 1965), and $N(M,\sigma)$ is a normal distribution with mean M and standard deviation σ. Numbers k_j^n, ω_n represent a sample of n wave-number vectors and frequencies of the modeled turbulence spectrum

$$E(k) = 16(\frac{2}{\pi})^{1/2} k^4 \exp(-2k^2) \tag{7}$$

3. Apply a scaling and orthogonal transformations to the flow-field v_i generated in the previous step to obtain a new flow-field u_i

$$w_i = c_{(i)}\, v_{(i)} \tag{8}$$

$$u_i = a_{ik} w_k \tag{9}$$

The procedure above takes as input the correlation tensor of the original flow-filed r_{ij} and information on length- and time-scales of turbulence (l, τ). These quantities can be obtained from a steady-state RANS computations or experimental data. The outcome of the procedure is a time-dependent flow-field $u_i(x_j, t)$ with correlation functions $\overline{u_i u_j}$ equal to r_{ij} and turbulent length/time scales equal to l, τ. As will be shown later this flow-field is also divergence free for a homogeneous turbulence and to a high-degree divergence-free for an inhomogeneous turbulence. By virtue of Eq.(4), spatial and temporal variations of u_i follow Gaussian distribution with characteristic length and time-scales of l, τ. Sampling for a different spectrum instead of Gaussian can also be used in different problems.

Equation (8), provides the scaling, and (9) - the orthogonal transformation. Scaling factors c_i obtained in step 1 represent the scales of turbulent fluctuations along each axis. They do not depend on time, whereas vectors v_i and w_i represent time-dependent velocity fluctuations. Both the scaling factors c_i and the transformation tensor a_{ij} are computed in step 1 using efficient matrix diagonalization routines that can be found in standard libraries or programmed specifically for a 3D case to boost the performance. By construction, the correlation tensor of the flow-field produced by Eq.(4) is diagonal

$$\overline{v_i v_j} = \delta_{ij} \tag{10}$$

The flow-field w_i produced after the scaling transformation (8) is divergence free for a homogeneous turbulence and nearly divergence free for an inhomogeneous turbulence, as is shown by the following estimate

$$
\begin{aligned}
w_{i,i} \;&=\; c_{i,i}\, v_i \;+\; c_i\, v_{i,i} \;\approx\; c_i\, v_{i,i} \;= \\
&= \frac{c}{l}\sqrt{\frac{2}{N}} \sum_{n=1}^{N} [-p_i^n\, k_i^n \sin(\frac{c}{c_j} k_j^n\, \frac{x_j}{l} \;+\; \omega_n \frac{t}{\tau}) \\
&\quad + q_i^n\, k_i^n \cos(\frac{c}{c_j} k_j^n\, \frac{x_j}{l} \;+\; \omega_n \frac{t}{\tau})] \;=\; 0 \qquad (11) \\
&\quad \Longrightarrow \;\; w_{i,i} \;\approx\; 0 \qquad (12)
\end{aligned}
$$

where we neglected all derivatives of c_i, which are slowly varying functions of $\vec{x}$, and used the relation of orthogonality between k_i^n and $p_i^n,\, q_i^n$

$$k_i^n\, p_i^n \;=\; k_i^n\, q_i^n \;=\; 0$$

which follows from the way vectors $p_i^n,\, q_i^n$ are constructed in (6). For a homogeneous turbulence the approximate equality in (11) will become a strict equality, leading to a divergence free flow-field. In the case of inhomogeneous turbulence the justification for neglecting the derivatives of c_i comes from the fact that c_i are derived from the correlation tensor r_{ij}, which is produced by the time-averaging operation in (1). As a result of this averaging r_{ij} is independent of time and may be a slowly varying function of space as compared to the fluctuating velocity u_i

$$\|c_{i,j}\| \;\approx\; \|r_{ij,k}\|^{1/2} \;\ll\; \|u_{i,j}\| \qquad (13)$$

where $\|\cdot\|$ denotes an appropriate function norm. Relation (13) justifies the first approximate equality in (11), leading to an approximate satisfaction of continuity.

The orthogonal transformation (9) preserves the solenoidal (divergence-free) property of the flow-filed

$$u_{i,i} = a_{ij} a_{ki} w_{j,k} = \delta_{jk} w_{j,k} = w_{j,j} = 0 \qquad (14)$$

where we used relation (12) and the rule of transformation of derivatives: $f'_{,i} \;=\; a_{ji} f_{,j}$. Thus, the generated flow-filed u_i is divergence-free within the accuracy determined by (13). At the same time the new flow field satisfies the anisotropy of the original flow-field $\vec{u}(\vec{x}, t)$, i.e.

$$
\begin{aligned}
\overline{u_i u_j} \;&=\; \overline{a_{im} w_m\, a_{jn} w_n} \;= \\
a_{im} a_{jn} \overline{w_m\, w_n} \;&=\; a_{im} a_{jn} c_m c_n \overline{v_m\, v_n} \;= \\
a_{im} a_{jn} c_m c_n \delta_{mn} \;&=\; a_{im} a_{jn} \delta_{mn} (c_n)^2 \;=\; r_{ij} \qquad (15)
\end{aligned}
$$

Where we used relations (3), (8) and the last equality was obtained by solving (2) for r_{ij}. Thus, the obtained flow-field $u_i(\vec{x}, t)$ is transient, divergence-free, inhomogeneous, and anisotropic with the pre-defined correlation coefficients.

Considering the flexibility and computational efficiency of the algorithm, we should note that the random spectrum sampling in Eq.(6) can be performed separately from the actual assembly of the vectors in Eq.(4). This leads to a higher computational efficiency, since the spectrum sampling can be done outside of the main time iteration loop of the flow solver with only the assembly of fluctuating velocity components left inside the time loop. This efficiency comes at a price of extra memory requirements for storing the random sample. The size of this sample is equal to $10 \cdot N$, where N is the number of harmonic functions representing the turbulent spectrum in (4), which is independent of the actual grid size. So, for $N = 1000$ and double precision arithmetics only $80\,KB$ of computer memory will be needed to store the spectrum for any grid size. This offers a flexibility of shifting the priorities between the high-accuracy spectrum generation and speed.

The RFG procedure can be extended to include the anisotropy of turbulence length-scale. In this case instead of using a scalar value for l in (5) one can define a vector l_i. An appropriate re-scaling would be necessary to preserve the continuity of the flow-field. This can be done by introducing another scaling transformation, similar to (8), which will guarantee that the resultant flow-field is divergence-free.

It should be noted that the turbulent flow-field obtained by the RFG procedure does not represent the solution of a complete Navier-Stokes (NS) equation, but rather of a continuity equation only. This is not a severe limitation, since the procedure is used mainly in the context of unsteady 3D computations, like LES, to generate initial or inlet boundary conditions. These conditions are given on three-dimensional subsets of a four-dimensional computational domain: two space and one time dimension for the inlet flow-filed and three space and zero time dimensions for the initial flow-field. As such these flow-fields do not have to satisfy the NS equation, since for an unsteady LES this equation is defined on a four-dimensional, 3-space $\times$ 1-time domain. However, the boundary conditions should be reasonably continuous, so that the NS solver will gracefully adjust the solution to the boundary conditions within the computational domain. This is exactly what the RFG procedure is designed to do. In addition to this it provides the desired statistical characteristics of turbulence at the boundaries, like anisotropy and inhomogeneity, which is of importance for LES and unsteady particle-dynamics computations.

Naturally, this approach to generate the inlet/initial boundary conditions is an approximation and should be used only when the statistical features of turbulence at the boundaries are of special concern while the solution of a full unsteady NS equation beyond the given boundaries is a practical impossibility.

3 Validation of RFG procedure

The first test of the procedure was for a homogeneous isotropic flow field. The Fourier space was sampled with 1000 wave-numbers selected according to Eq. (4). Figures 1(a),1(b) shows the snapshot of a homogeneous isotropic velocity field. Fig.1(a) shows the vorticity field in a cross-section of the computational domain, and in Fig.1(b) the velocity distribution is presented. Statistical post-processing of velocity correlations was applied to the generated flow-field in order to verify that the velocity field was isotropic. For this purpose a turbulent flow-field with the characteristic time scale of $10^{-3}\,s$ was generated from the Fourier spectral sample of 1000 wave-vectors (Eq.4). The fluctuating velocities were sampled at the rate of $10^5\,Hz$. Correlations of the fluctuating velocity components were computed at one point in space by averaging over time. Fig.4 shows the behavior of the velocity correlations as a function of the averaging time-interval. The figure indicates convergence to the values corresponding to Eq.(10).

The procedure was next applied to a homogeneous anisotropic flow field with c_i selected from typical boundary layer distributions. This type of anisotropy leads to higher amplitudes of the velocity vectors in one direction relative to the other (Fig.1(c)). The procedure was also used to generate the flow-field with anisotropic length-scales (see comments in Sec.2). In this case the length-scale of fluctuations was selected differently in different spatial directions. This produced a flow-field where the structure of the velocity fluctuations seemed stretched in one direction (Fig.1(d)).

Next we applied the procedure to the case of a non-homogeneous anisotropic boundary layer. Figure 1(e) shows a snapshot of the velocity magnitude in the three-dimensional boundary layer. An additional empirical factor related to the boundary-layer thickness was introduced in this case to better account for the intermittency effects. Figure 2 shows the random signal produced by the RFG procedure sampled at different locations above the boundary plane. As can be seen from that figure both anisotropy and inhomogeneity are evident in the fluctuating components. Experimental and direct numerical simulation (DNS) data do exist for this flow field, providing both mean and fluctuating velocity profiles, as well as turbulent correlations. The turbulent boundary layer is two-dimensional in the mean, though turbulent fluctuations exist in all three dimensions, i.e. $c_1 = u'$, $c_2 = v'$, and $c_3 = w'$ for the axial, vertical, and tangential directions, respectively. In addition, the correlation involving the axial and vertical velocity fluctuations is significant. The Reynolds stresses were obtained from (Hinze, 1975) where the classical experiments of Klebanoff (1954) are summarized.

A number of realizations N_T of the boundary layer was computed using the turbulence time scale of $t_{turb} = 10^{-3}\,s$, length-scale of $l_{trub} = 10^{-3}$, and a sample size of 1000 harmonic functions. The wave-vectors for these functions were taken from a normal distribution with the mean $\sim t_{turb}^{-1}$. The boundary layer thickness (δ) was allowed to grow according to the following empirical relation:

$$\delta \;=\; 0.16 \cdot \; x \cdot \left(\frac{U_0 x}{\nu}\right)^{-1/7} \;=\; 0.16 \cdot \; x \cdot \; Re_x^{-1/7} \tag{16}$$

where x is the axial distance and U_0 is the free-stream velocity, which was set equal to $1.0\,m/s$. The cross correlation ($\overline{uv}$) was normalized with the friction velocity U_τ, which is itself a function of U_0. The boundary layer thickness was randomly perturbed with a continuous function using the same spectral sampling technique as for the velocity fluctuations to emulate intermittency.

Fig.3 shows the vorticity field of the generated boundary layer flow-field compared with LES data (Speziale, 1998). As can be seen from the figure, by choosing the turbulence length-scale correctly, one can achieve a good resemblance in the flow structure simulated with this semi-analytic approach and a LES flow-field.

To compare the simulation results with the experimental data the velocity profile along a vertical line in the center of the axial plane was stored for each simulated realization of the flow-field. The profiles of the thousand time realizations were then used to calculate the average fluctuating components in each direction, as well as the corresponding cross correlations. These are compared to the original experimental data in the Figure 5. As can be seen, the experimental data is well reproduced.

The divergence-free property of the generated flow-filed was tested by computing the divergence as a function of turbulence length-scale for three cases: isotropic velocity field, generated according to the original Kraichnan method (Kraichnan, 1970; Li et al., 1994), anisotropic velocity field, generated according to the modified Kraichnan method, using Eqs.(4)-(5) with $\tilde{k}_j^n \equiv k_j^n$, and anisotropic velocity field generated according to the RFG algorithm based on Eqs.(2)-(9). For this test case the anisotropy of different fluctuating velocity components was selected to be given by a ratio: $0.1 : 1.4 : 1$ for c_1, c_2, and c_3 respectively.

The divergence test was done on a cubic grid. For each grid-cell the divergence was computed as the sum of fluxes through cell faces. The Fourier space was sampled with 1000 wave-numbers selected according to Eq. (4). Fig.6 depicts the computed divergence as a function of the ratio of turbulence length-scale l to grid cell size. The result represents an average over 10,000 realizations of the flow-field. As can be seen from the figure in all three cases the continuity error decreases with the increase of the turbulence length-scale. This decrease is considerably slower for the anisotropic flow-field generated according to the original Kraichnan method compared with the the cases of isotropic flow field and anisotropic flow generated with RFG procedure. It should be noted that the theoretical continuity error in the isotropic case is zero. The discrepancy between this case and the anisotropic case computed with the Kraichnan method is due to the violation of continuity of that method in the presence of anisotropy. In contrast, the flow-field produced with the new RFG procedure has practically the same as for the isotropic case. This means that the anisotropic flow-field generated by the RFG procedure is essentially divergence free. At the same time is shows the importance of scaling transformation for k_j^n in (5) for the fulfillment of continuity. The upper divergence limit in the figure occurs when the grid cell-size is comparable or greater than turbulence length-scale l. It is due to the integration errors, which in this limit case can be estimated from the relation $\|\overline{u_i u_j}\| \approx 1$.

Another validation of the method was done on a flat-plate wake flow, which is a well

documented case in the literature (Ramaprian et al., 1981). In this case the simulation starts from a plane located behind the plate in the wake region (Fig. 7). The inflow boundary is generated using RFG with an input from the experimental data (Ramaprian et al., 1981), including mean velocity U_m, the turbulence intensities $u_{rms}, v_{rms}, w_{rms}$ and the shear stresses $\overline{uv}$. In this way we can provide realistic inflow boundary conditions including the turbulence characteristics created by the plate, which is an important factor for LES. The length of the plate is $L = 1.829m$. The inflow boundary is located at $19.5mm$ ($x/L = 0.01$) measured from the rear edge of the plate. The computational domain size is $1.0m \times 0.2m \times 0.6m$ in x,y and z direction, respectively. The corresponding grid sizes are $82 \times 50 \times 50$. Non-uniform grid is used in both x and y directions with stretching not exceeding three percent[2]. The size of the smallest cell is $0.6mm \times 0.2mm \times 1.2mm$ while that of the biggest cell is $50mm \times 8mm \times 1.2mm$ in x, y, z direction, respectively. Neumann boundary condition is applied at the outflow boundary. Symmetry boundaries are used in a vertical direction and periodic boundaries are used in the span-wise direction. Central difference numerical scheme and Smagorinsky model are applied in this study.

Fig.8 presents the comparison of the turbulent characteristics between the simulation and the experimental results at the inlet plane. They are agreed very well except the center region. The reason is that the grid is relatively coarse in the center, which leads to the smoothing of very sharp gradients. The overall difference is under 1%. It should be noted that the agreement is so good because the comparison is given for the inlet plane where the RFG procedure was designed to reproduce the turbulence quantities exactly.

Fig.9(a) shows the energy spectrum at the inflow boundary. A sharp cut exists at wave length 0.01, which is matching the length scale we selected for RFG. Fig.9(b) and Fig.9(c) show the energy spectrum at $x = 0.16$ and $x = 0.53$ respectively, which were produced after the application of LES inside the domain. From these figures, one can see that a good portion of the inertial range is captured. With the grid becoming coarser in the wake, only large wave lengths can be resolved.

Next we investigated the turbulence intensities downstream. From Fig.10 to Fig.13 the Reynolds stresses computed along y- direction at different x locations are compared with the experimental results. The comparison looks good although more quantitative studies would be appropriate. Near the very beginning of the wake most of the fluctuations can be captured. Later in the flow field, the percentage of the resolved turbulence is becoming small due to the coarser grids. It can be noted that both $v^{'}$ and uv at the second x-station are higher than those at the first one. This effect has been investigated and discussed by Nakayama and Liu (1990) where they attribute it to a near wake phenomenon. Figure 14 shows the decay of the turbulent kinetic energy along the center line of the wake. Most part of the turbulent kinetic energy has been captured. We are confident to make an assumption that with finer grids the turbulent resolution will be much better.

[2] In this study, x represents stream-wise, y - vertical and z - span-wise directions, respectively

4 Applications

4.1 Boundary conditions for LES/RANS

As an illustration of the technique we used it first in conjunction with the RANS and LES methods to simulate turbulent fluctuations in a ship wake. The high-Reynolds number character of ship wakes ($R_e \sim 10^7 - 10^8$) makes it rather time-consuming to perform full-scale LES of these flows. In this situation a combination of a RANS and the RFG technique can offer an efficient way to restrict the LES runs to the wake region only.

Figure. 15 shows a snapshot of an unsteady turbulent flow-field in the inflow-plane serving as inlet condition for LES of a ship wake. Initially a steady state RANS solution is obtained (Figs.15(a),15(c)), providing turbulent stresses r_{ij} and time-scales ω_i. Next the RFG procedure is used to generate continuous time-dependent inlet conditions with the given turbulence characteristics (r_{ij} , ω_i, Figs.15(b), 15(d)).

In another application (Fig. 16) turbulent flow around a ship-hull was produced as a superposition of the mean flow velocity, computed with a RANS method ($k - \epsilon$) (Larreteguy, 1999) and the fluctuating velocity obtained with the RFG procedure. This flow-field can be used to initialize the unsteady LES and for particle tracking applications (see Sec. 4.2).

As noted earlier, the flow generated in both cases may not necessary represent a realistic turbulent vortex dynamics at the respective boundaries, but statistically the flow-field will reproduce the turbulent shear stresses and time/length scales correctly. Furthermore, the statistics of turbulent fluctuations imposed at the space/time boundaries may not necessary be preserved by the flow-solver inside the domain. That is, there may be a transition region between the boundary and the inside of the domain where the flow-solver will adjust to the boundary conditions. However, if the boundary conditions were generated using continuous functions and realistic turbulence quantities and spectra this transition region will be small and the technique may still present a good alternative to solving the complete NS equation in a larger computational domain.

4.2 Particle dynamics modeling

Particle tracking in transient flows is usually a time-expensive computational procedure. In the situations when the turbulent flow is computed using RANS models it is possible to compute particle dynamics in a steady-state mean flow field and add a fluctuating component to particle velocities. When LES technique is used particles should follow a time-dependent flow-field and the fluctuating component should still be added to it at smaller turbulence scales. In both cases the fluctuating component is derived from the turbulence intensity and length-scales, provided by the turbulence model.

4.2.1 Bubble-dynamics in a turbulent flow

We shall continue with a ship-wake flow as an illustrative example of particle-tracking application in turbulent high-Reynolds-number flows. Simulations of bubbles in ship wakes requires account of several processes, like drag, lift and buoyancy forces, bubble dissolution in water, bubble interaction with the free-surface (including bubble disappearance at the surface and bubble generation due to air entrainment). In some cases, because of uneven bubble distribution (e.g. local clustering), the coalescence and/or breakup of bubbles may be important. Because of this non-uniformity, sharp gradients in bubble concentration, and low volume fraction of the bubbles Lagrangian approach to model bubble dynamics is often preferred. Compared to the two-fluids method (Elghobashi, 1994; Crowe, 1998) the Lagrangian approach requires less empiricism and is more suitable for parallel implementation. We use a particle dynamics (PD) algorithm based on efficient particle tracking, population dynamics and a novel particle interaction techniques (Smirnov et al., 2000).

To simulate bubbles in a ship-wake we use the combination of RFG and PD algorithms. Fluid velocity at the location of every bubble was approximated as a sum of the mean fluid velocity obtained from the RANS calculations and the fluctuating part computed with the RFG procedure. Since RANS solution is given only at the Eulerian grid-node locations and bubbles follow Lagrangian trajectories, an interpolation is required to approximate the mean velocity at bubble's current location. No such approximation is necessary for the fluctuating part, since the RFG procedure defines a flow-field at every point in space and time. In the simulation the bubbles were injected at a single point close to the ship hull where the turbulent kinetic energy was near its maximum (Fig. 17). Drag, buoyancy and added-mass terms were included (Crowe et al., 1998). A total of $10\ 000$ bubbles of 100 microns in diameter were continuously injected into the domain. Two seconds of real-time were simulated for the ship-length of $6m$ traveling with the speed of $3m/s$. The figure shows the tendency of particles to agglomerate in dense groups. The characteristic sizes of these groups are in many instances smaller than the grid-cell size. This reflects the very sub-grid nature of the RFG method, which enables to capture finer details of particle dynamics than can be resolved on an Eulerian grid.

4.3 Large-Eddy Simulations (LES)

In Large Eddy Simulations the RFG procedure can be used to generate random inflow-conditions or serve as a subgrid-scale model. There is an extensive literature regarding LES techniques (Piomelli, 1999). To reach a state of developed turbulence in LES simulations require a substantial computational time. Regarding this there are two important problems in LES of a high-Reynolds number turbulence that can be solved with the RFG procedure: (1) assigning initial flow-field distribution and (2) assigning turbulent inflow conditions. Conventionally, the first problem is dealt with by increasing the transition phase of the simulation and the second - by extending the size of the

computational domain. Consequently, the remedy comes at a price of a longer execution time and higher memory requirements. By using a RFG procedure to generate the initial conditions one can cut down on the execution time considerably. For stationary turbulence the approximate nature of the initial velocity distribution with respect to the solution of the NS-equation is of little significance, since these discrepancies are corrected in the first few iterations of the NS-solver.

The problem of inlet conditions could be even more important, since extending the computational domain will increase both execution time and memory requirements of the simulation. In this case RFG can provide reasonable inflow conditions with the predetermined anisotropy properties. Here again we illustrate these advantages on the example of a ship wake. A complete LES simulation of the wake would normally require simulating the unsteady flow around the ship hull and in the wake region. Employing the RFG procedure for the inlet conditions, we can restrict LES run to the wake region only. In this case the information on turbulence levels and anisotropy at the inlet plane, required by RFG, can be obtained from relatively inexpensive RANS calculations.

After validating this approach on the case of a flat-plate (see Sec.3), we applied it to the wake of a model ship (Navy 5415 model (Carrica et al., 1998)). As in the flat-plate case the inflow boundary was constructed using the data from RANS calculations (Larreteguy, 1999) (Fig.15). The turbulent normal stresses are based on the kinetic energy. The time scale and length scale which are used in generation of the perturbation at the inlet plane are selected from the corresponding relation between the turbulent kinetic energy and its dissipation rate provided by the RANS calculations.

Figure 18 shows the instantaneous stream-wise velocity contours and vertical vorticity contours, respectively, in a plane parallel to the free surface, where some of the the turbulence structures in the wake can be observed. Small-scale turbulent structures can be seen in both figures in the near wake region. These structures tend to increase in the far wake. This can be due to the following two factors: (1) In the very near wake, fine grids are applied so that smaller turbulence structures are captured. (2) Physically, larger turbulence structures include more energy so that they can last longer, while smaller turbulence structures have less energy and die quickly by dissipation. Another phenomenon is the increase of the width of the wake in the downstream direction. The mean velocity profile (not shown here) also supports this result. Capturing of these phenomena testifies to the validity of our approach of computing the inflow boundary.

5 Conclusions and future work

The analytical method of Kraichnan (1970) was modified to account for the effects of inhomogeneity and anisotropy of turbulent shear stresses. The technique was realized in an efficient random field generation (RFG) algorithm which was tested on the cases of isotropic turbulence, channel flow anisotropic flows, boundary layer inhomogeneous anisotropic turbulence (Celik et al., 1999) and flat-plate wake flow. The simulated flow

fields are transient in nature and satisfy the conditions of continuity and anisotropy for homogeneous flows and to a good approximation satisfy these conditions for inhomogeneous flows.

The RFG procedure offers a relatively inexpensive way to generate random velocity fluctuations, representing a turbulent flow-field. Since the generated velocity field satisfies the relations of continuity and anisotropy it is a far more realistic representation of turbulence than can be obtained with a simple Gaussian velocity distribution using a random-number generator. Because the flow-field produced by RFG may not satisfy the momentum equations it is still an approximation. However, in some applications this approach may offer a simple and reasonably accurate way to model turbulence without solving the complete Navier-Stokes equation, which would require much more memory and execution time.

In practical applications the RFG procedure provides the flexibility of a trade-off between the accuracy of representing a turbulent spectrum and memory/time requirement. By increasing the spectral sample size N in (4) one can increase the accuracy of reproducing the turbulent spectrum at the cost of longer execution time and higher memory utilization. In addition to that, since the velocity field is calculated by analytical functions it is given at any point in space and time, and not just at the grid nodes and at discrete time values. Because of this quality, the method has a potential as a subgrid-scale model for LES or RANS simulations and in modeling turbulent particle-laden flows, although its validity in this respect would require a separate study.

Advancing the realistic LES run to the stage of developed turbulence may require days of computation time[3]. Similarly, to obtain realistic turbulent inflow conditions may require the extension of the computational domain with the corresponding increase in computer time and memory requirements. The RFG technique can reduce the flow initialization time to several hours and can be used to continuously supply the turbulent inlet conditions close to the domain of interest, thereby reducing time and memory requirements of the LES simulations.

This study showed the feasibility of applying a hybrid LES technique in combination with RFG algorithm to high-Reynolds number flows, like those of ship wakes. It is also shown that the technique can be used effectively in conjunction with a Lagrangian particle dynamics approach, is appropriate for bubble tracking in the wake and can be easily incorporated into LES codes.

Acknowledgments:

This work has been performed under a DOD EPSCoR project sponsored by the Office of Naval Research (ONR), Grant No.N00014-98-1-0611. The program officer is Dr. Edwin P. Rood. We thank professor Robert Street of Stanford University who kindly provided us with the basic code for LES. We also thank Dr.Calhoun and Mr.Li Ding in Stanford University for their suggestions about using the code.

[3] Our benchmarking was performed on the 533 MHz DEC-Alpha processor

References

Akselvoll, K. and Moin, P.: 1995, Technical Report TF-63, Stanford University

Bechara, W., Bailly, C., and Lafon, P.: 1994, Stochastic approach to noise modeling for free turbulent flows, *AIAA Journal* 32(3)

Carrica, P., Bonetto, D., Drew, D., and Lahey, R.: 1998, The interaction of background ocean air bubble with a surface ship, *Int.J.Numer.Meth.Fluids* **28**, 571

Celik, I., Smirnov, A., and Smith, J.: 1999, Appropriate initial and boundary conditions for LES of a ship wake, in *3rd ASME/JSME Joint Fluids Engineering Conference*, Vol. FEDSM99-7851, San Francisco, California

Crowe, C.: 1998, An assessment of multiphase flow models for industrial applications, in *Proceeding of FEDSM'98*, Vol. FEDSM-5093, Washingtow,DC,USA

Crowe, C., Sommerfeld, M., and Tsuji, Y.: 1998, *Multiphase Flows with Droplets and Particles*, CRC Press

Elghobashi, S.: 1994, On predicting particle-laden turbulent flow, *Applied Scientific Research* **52**, 309

Ferziger, J.: 1983, Higher-level simulations of turbulent flows, in J. Essers (ed.), *Computational Methods for Turbulent Transsonic and Viscous Flows*, pp 93–183, Hemisphere Publishing Co., Springer Verlag

Fung, J., Hunt, J., Malik, N., and Perkins, R.: 1992, Kinematic simulation of homogeneous turbulence by unsteady random Fourier modes, *J. Fluid Mech.* **236**, 281

Hinze, J.: 1975, *Turbulence, 2nd edition*, McGraw-Hill, New York

Klebanoff, P.: 1954, *NACA Tech. Notes* 3133

Kraichnan, R.: 1970, Diffusion by a random velocity field, *Phys. Fluid* **11**, 43

Larreteguy, A.: 1999, *Ship-Wake simulations*, Private communication

Lee, S., Lele, S., and Moin, P.: 1992, Simulation of spatially evolving turbulence and the applicability of Taylor's hypothesis in compressible flow, *Physics of Fluids* **4**, 1521

Li, A., Ahmadi, G., Bayer, R., and Gaynes, M.: 1994, Aerosol particle deposition in an obstructed turbulent duct flow, *J. Aerosol Sci.* **25(1)**, 91

Lund, T.: 1998, Generation of turbulent inflow data for spatially-developing boundary layer simulations, *Journal of Computational Physics* **140**, 233

Maxey, M.: 1987, The gravitational settling of aerosol particles in homogeneous turbulence and random flow fields, *J. Fluid Mech.* **174**, 441

Nakayama, A. and Liu, B.: 1990, The turbulent near wake of a flat plate at low reynolds number, *J.Fluid Mech.* **217**, 93

Piomelli, U.: 1999, Large-eddy simulation: achievements and challenges, *Progress in Aerospace Sciences* **35**, 335

Ramaprian, B., Patel, V., and Sastry, M.: 1981, *Turbulent wake development behind streamlined bodies*, Technical Report IIHR Report No.231, Iowa Institute of Hydraulic Research, The University of IOWA

Ravikanth, V. and Pletcher, R.: 2000, *AIAA Paper* (2000-0542)

Shi, S., Smirnov, A., and Celik, I.: 2000, Large-Eddy simulations of turbulent wake

flows, in *Twenty-Third Symposium on Naval Hydrodynamics*, pp 203–209, Val de Reuil, France

Smirnov, A., Shi, S., and Celik, I.: 2000, Random Flow Simulations with a Bubble Dynamics Model, in *ASME Fluids Engineering Division Summer Meeting*, No. 11215 in FEDSM2000, Boston, MA

Spain, B.: 1965, *Tensor Calculus*, Oliver and Boyd

Speziale, C.: 1998, Turbulence modeling for time-dependent RANS and VLES: a review, *AIAA Journal* **36(2)**, 173

Zhou, O. and Leschziner, M.: Sept. 1991, A time-correlated stochastic model for particle dispersion in anisotropic turbulence, in *8-th Turbulent Shear Flows Symp.*, Munich

Zhou, Q. and Leschziner, M.: 1996, *Modelling particle Dispersion in Turbulent Recirculating Flow with an Anisotropy- Resolving Scheme*, Technical Report TFD/96/07, UMIST

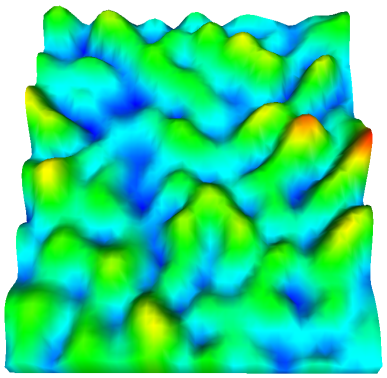

(a) Isotropic Vorticity

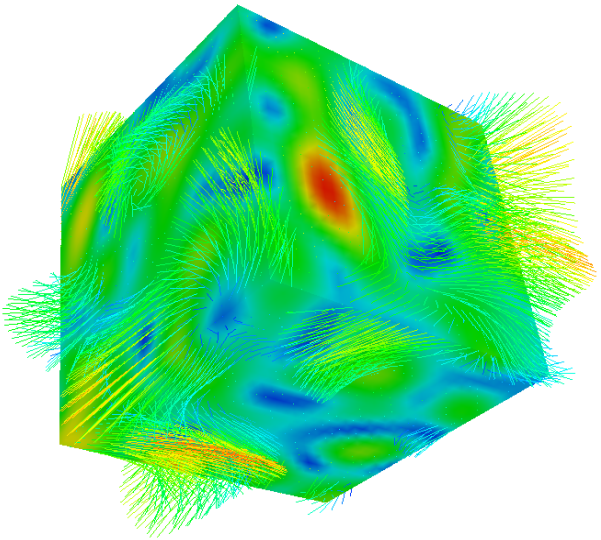

(b) Isotropic Velocity

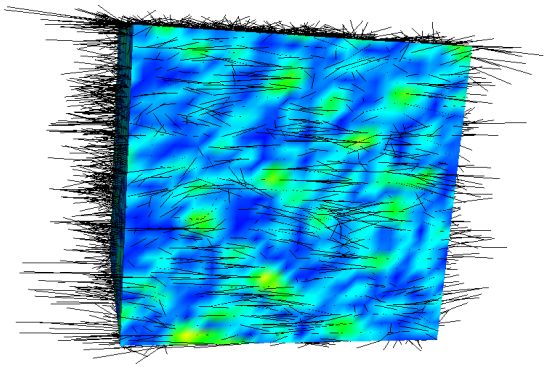

(c) Anisotropic velocity

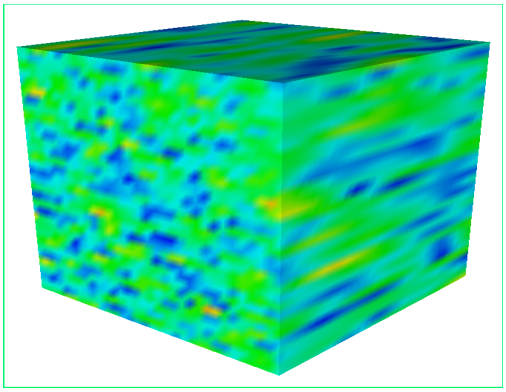

(d) Anisotropic length-scale

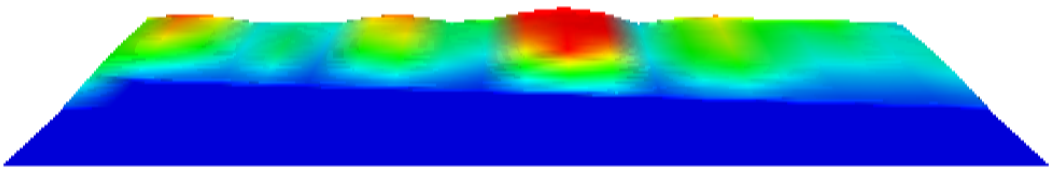

(e) Fluctuating velocity in the boundary layer

Figure 1: Simulated flow-field

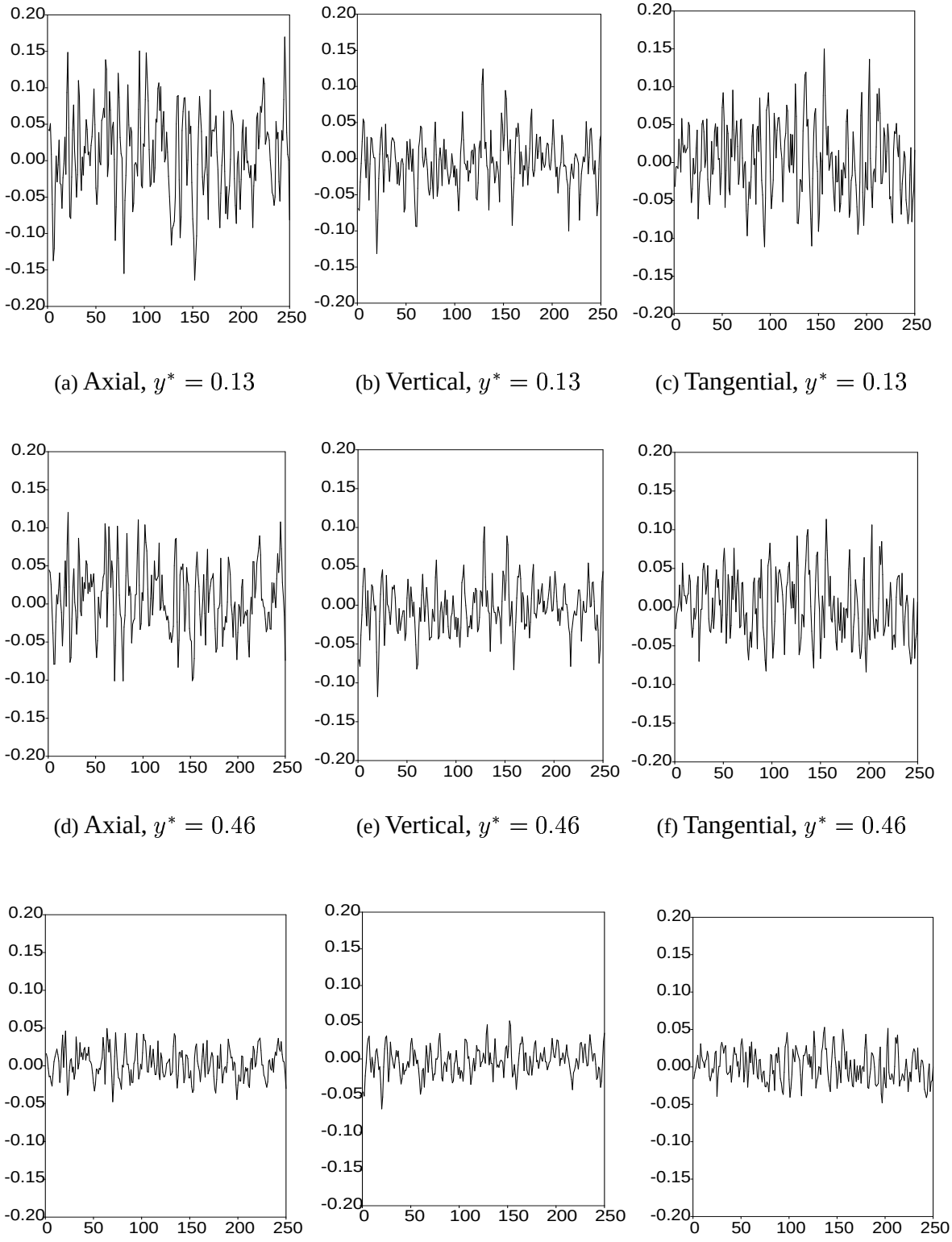

(a) Axial, $y^* = 0.13$ (b) Vertical, $y^* = 0.13$ (c) Tangential, $y^* = 0.13$

(d) Axial, $y^* = 0.46$ (e) Vertical, $y^* = 0.46$ (f) Tangential, $y^* = 0.46$

(g) Axial, $y^* = 0.76$ (h) Vertical, $y^* = 0.76$ (i) Tangential, $y^* = 0.76$

Figure 2: Instantaneous velocity vs time step at different locations, $y^* = y/\delta$

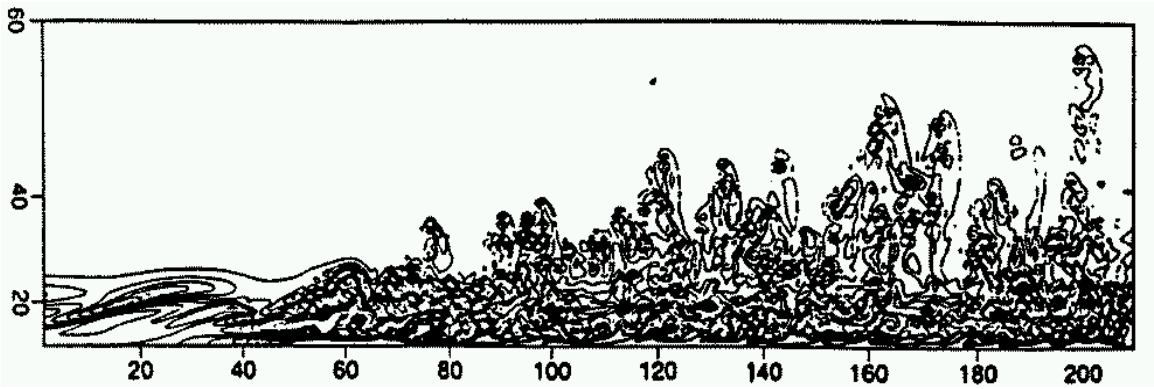

(a) LES (Speziale, 1998)

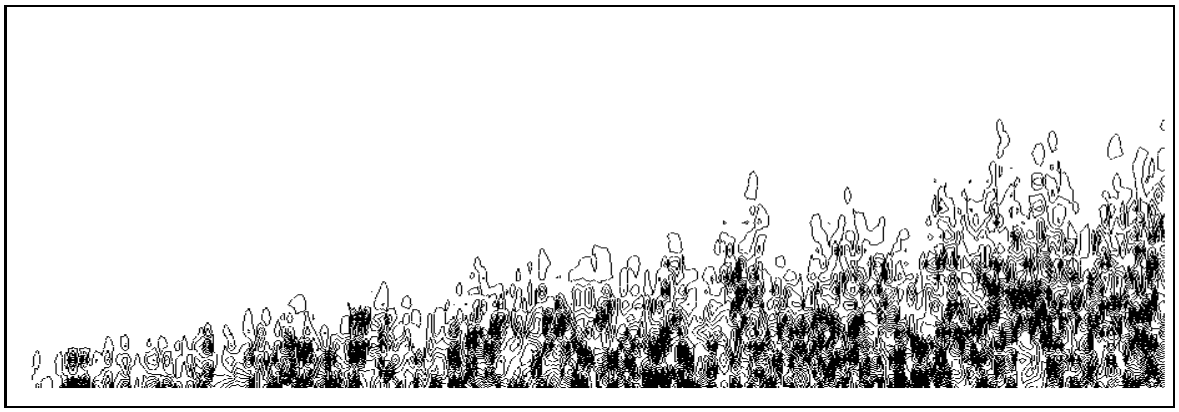

(b) RFG (large length-scale)

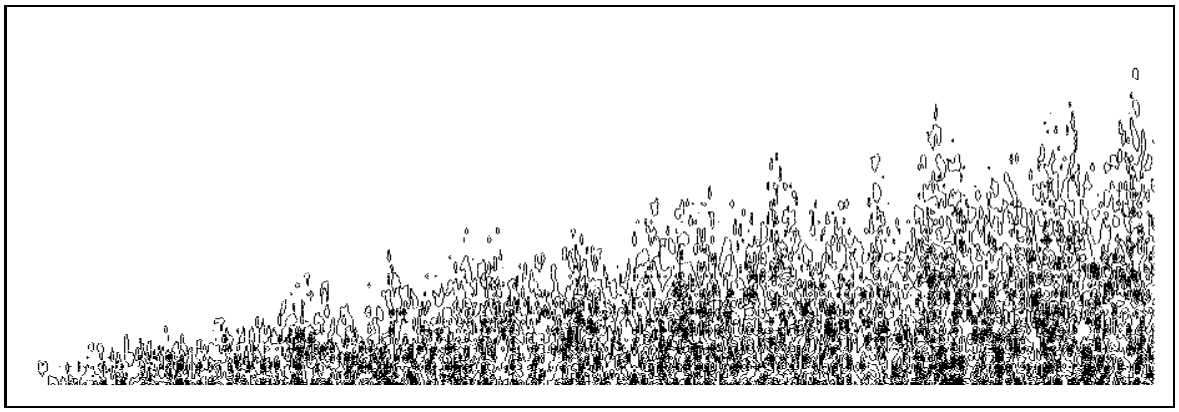

(c) RFG (small length-scale)

Figure 3: Vorticity contours in the boundary layer

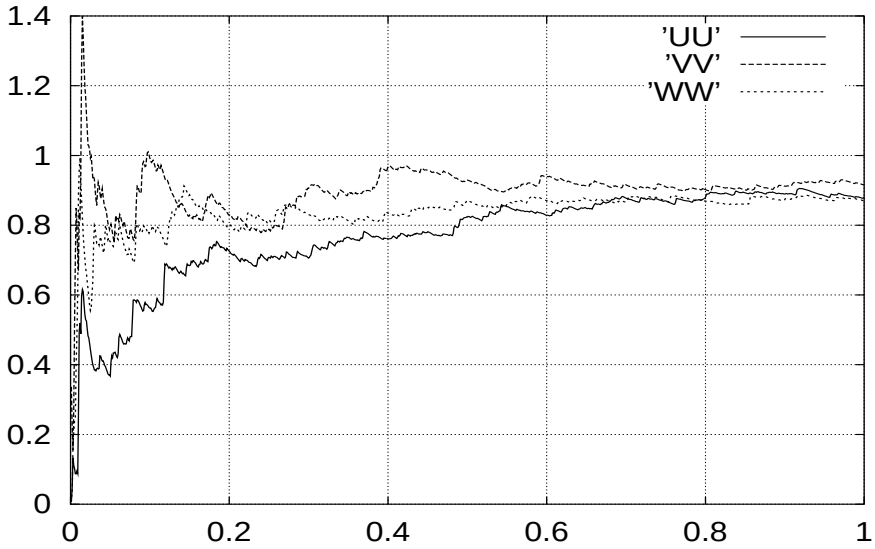

(a) Diagonal correlations

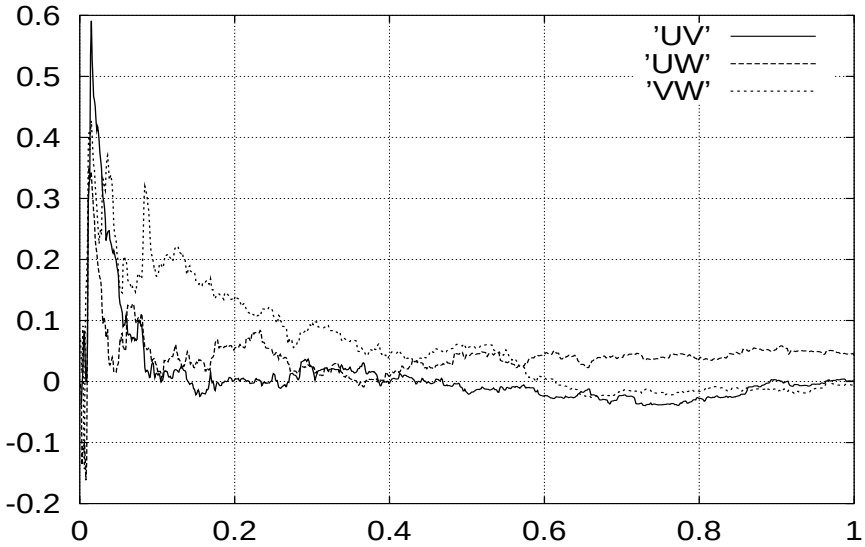

(b) Cross correlations

Figure 4: Convergence of velocity correlations

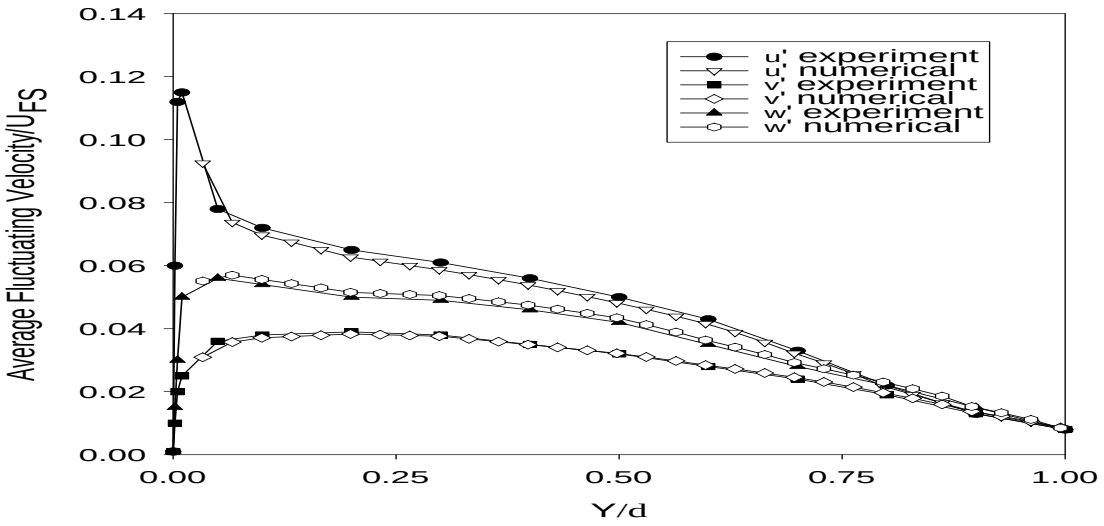

(a) Fluctuating velocities

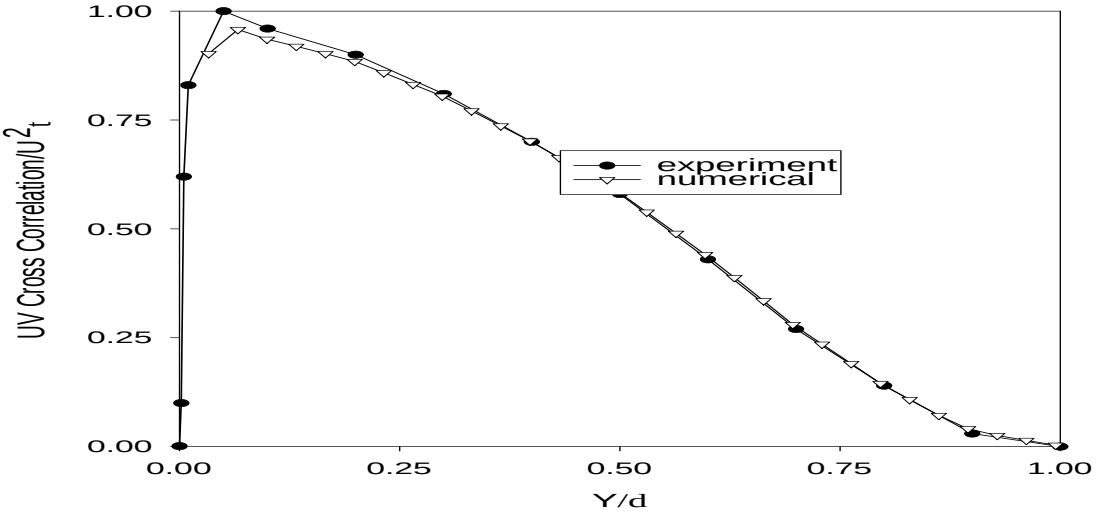

(b) Axial/vertical cross correlations

Figure 5: Comparison with experimental data

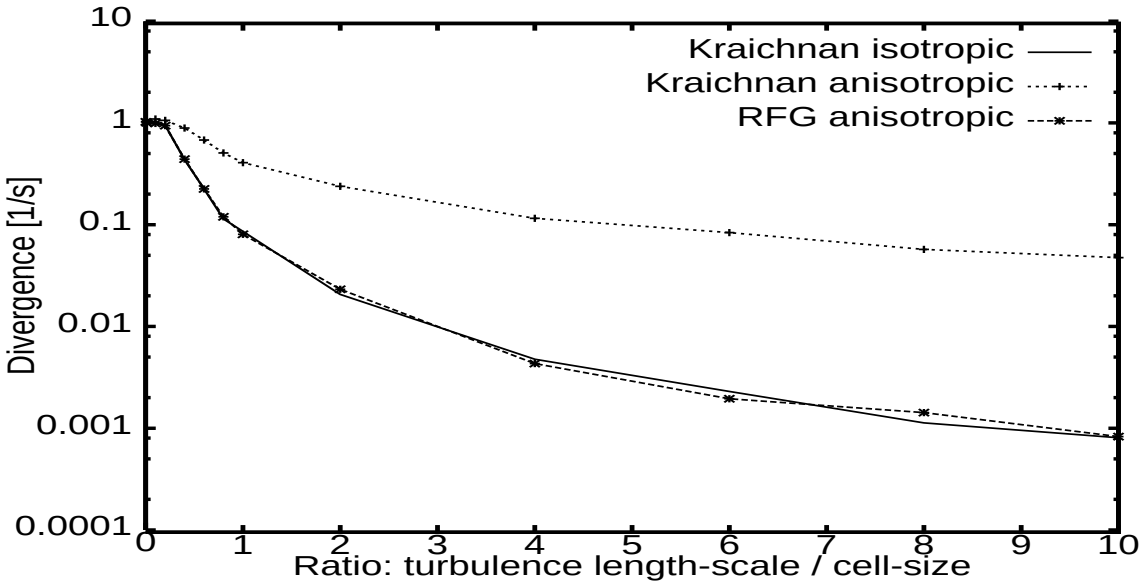

Figure 6: Normalized divergence of an anisotropic velocity field

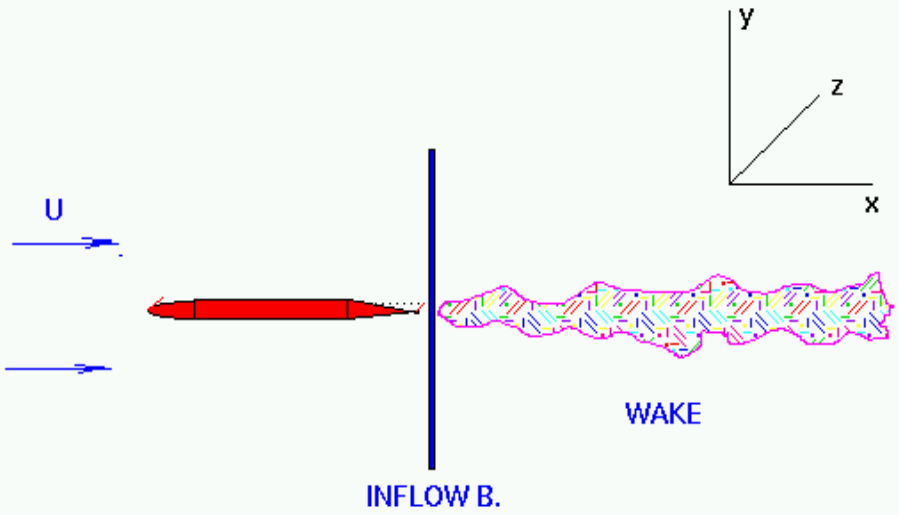

Figure 7: The schematic of the flat plate wake

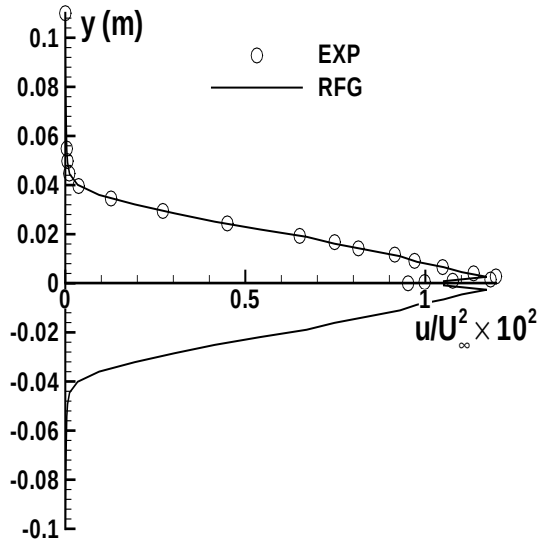

(a) Stream-wise, u_{rms}

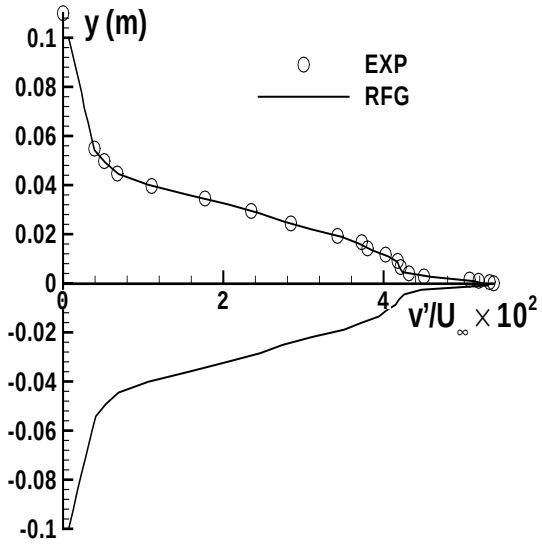

(b) Span-wise, v_{rms}

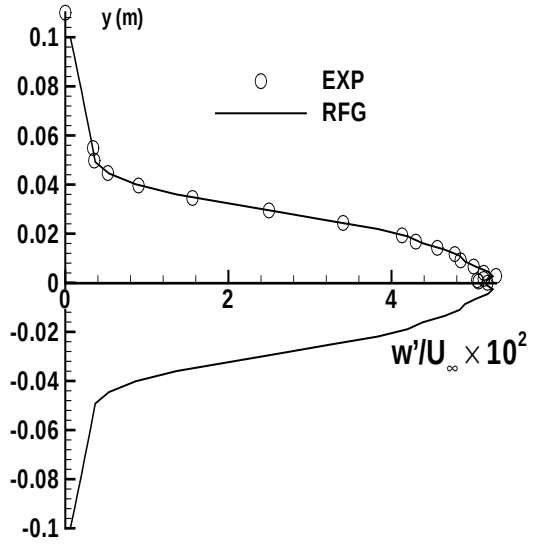

(c) Vertical, w_{rms}

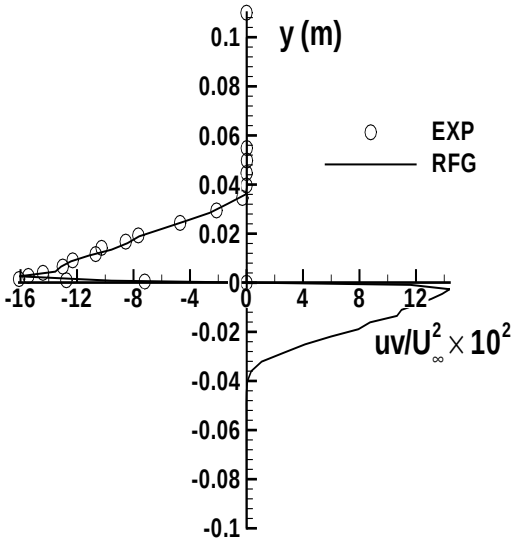

(d) Shear stress, uv_{rms}

Figure 8: Turbulence intensities at the inflow boundary.

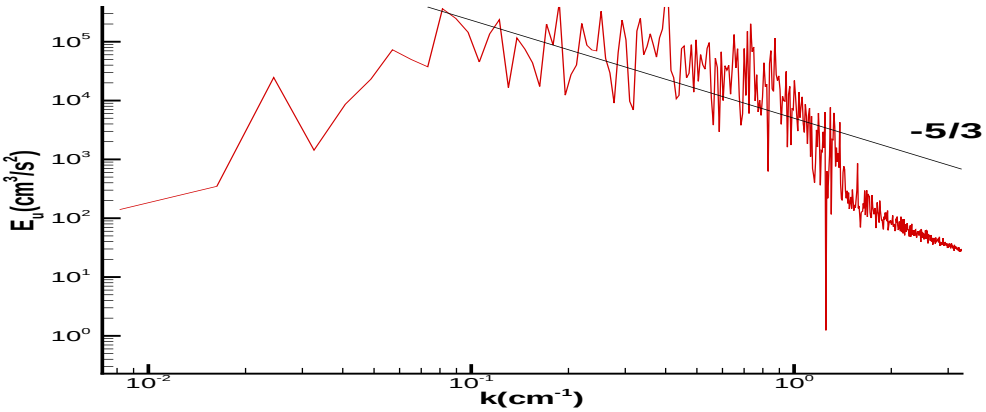

(a) Energy spectrum at the inflow boundary

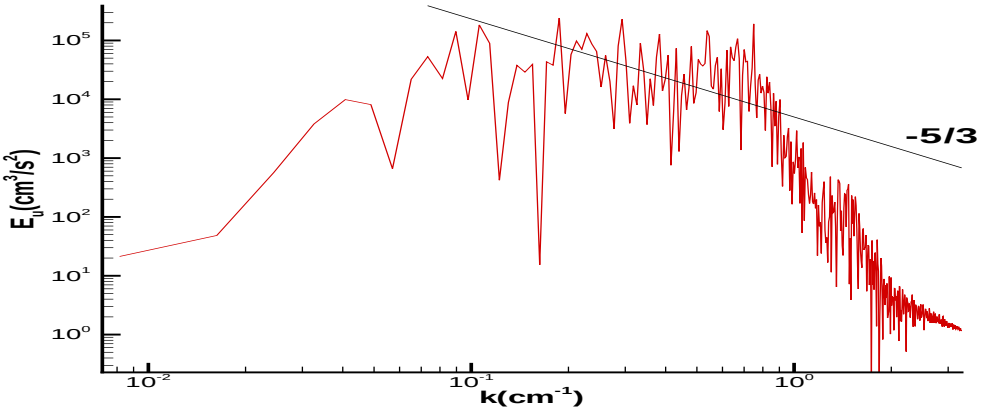

(b) Energy spectrum at x=0.16

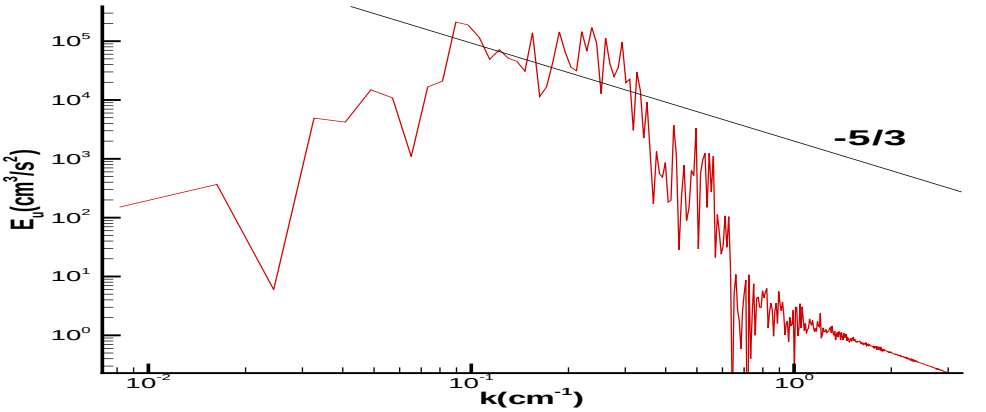

(c) Energy spectrum at x=0.53

Figure 9: Energy spectrum at different x locations

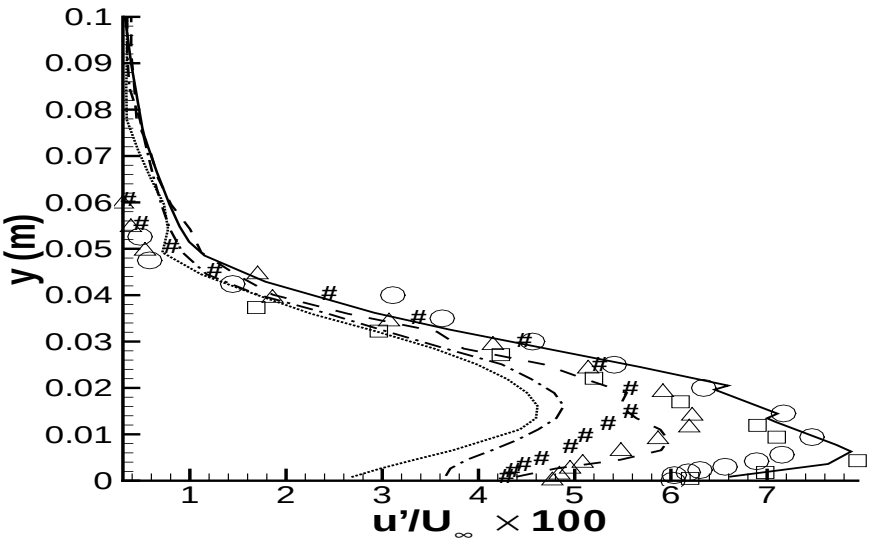

Figure 10: Comparison between simulation and measured turbulence intensity (u_{rms}). ——, present simulation results at $x = 31.75mm$; − − −−, present simulation results at $x = 158.75mm$; − · − · −, present simulation results at $x = 361.95mm$; · · · · ·, present simulation results at $x = 590.55mm$; □, Exp. results (Ramaprian, et al. 1981) at $x = 31.75mm$; ∘, Exp. results (Ramaprian, et al. 1981) at $x = 158.75mm$; Δ, Exp. results (Ramaprian, et al. 1981) at $x = 361.95mm$; #, Exp. results (Ramaprian, et al. 1981) at $x = 590.55mm$;

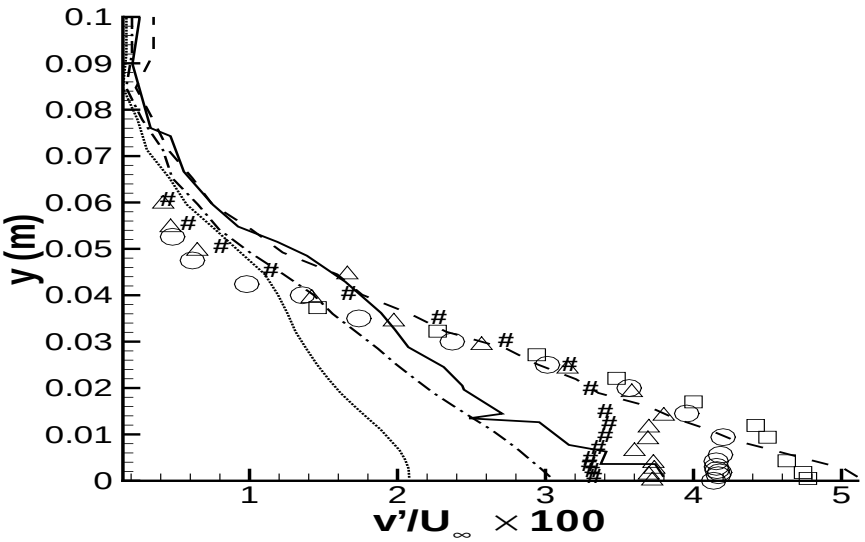

Figure 11: Comparison between simulation and measured turbulence intensity (v_{rms}). The symbols are the same as Fig.10

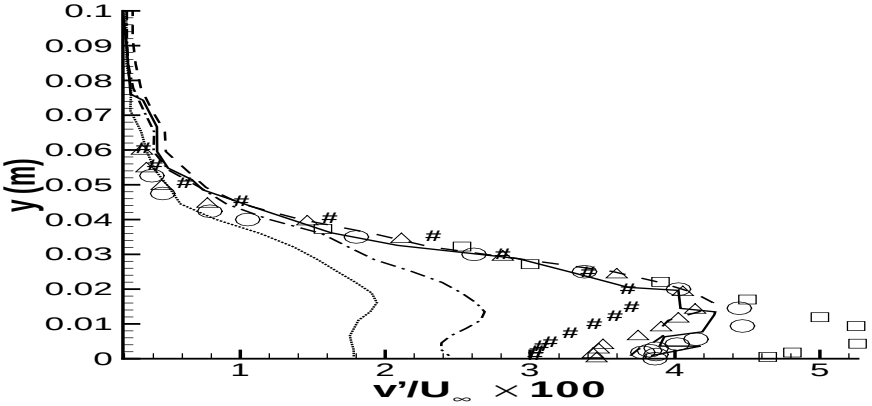

Figure 12: Comparison between simulation and measured turbulence intensity (w_{rms}). The symbols are the same as Fig.10

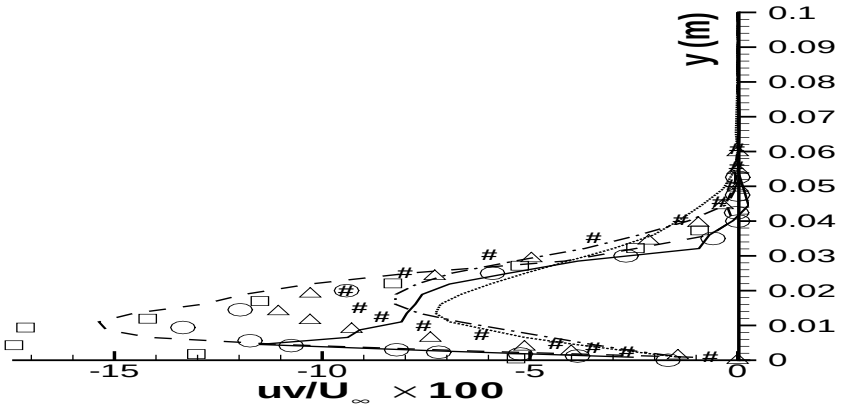

Figure 13: Comparison between simulation and measured shear stresses The symbols are the same as Fig.10

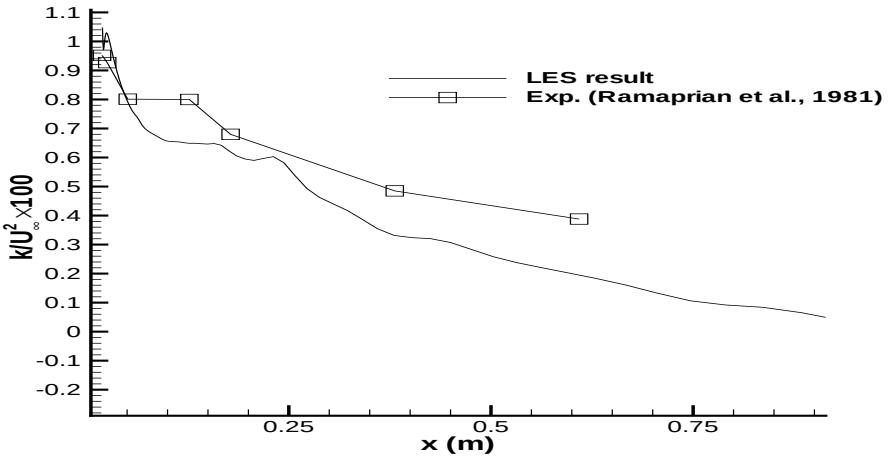

Figure 14: Kinetic energy profile along the center line in the wake of a flat plate

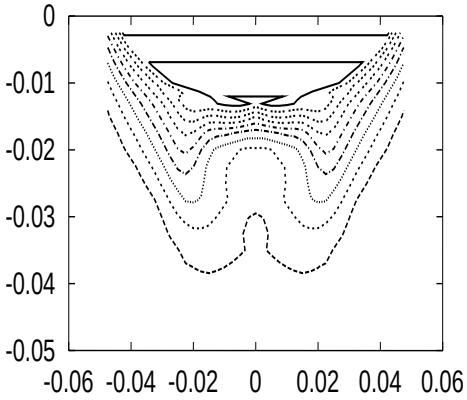

(a) Streamwise (RANS)

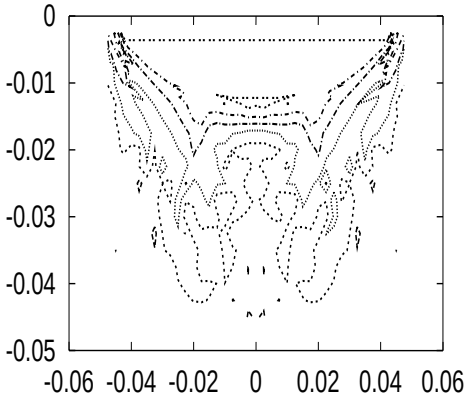

(b) Streamwise (RANS+RFG)

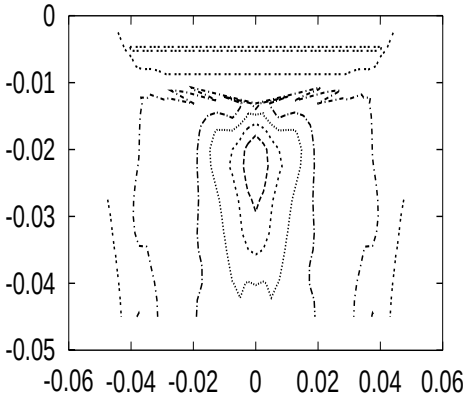

(c) Vertical (RANS)

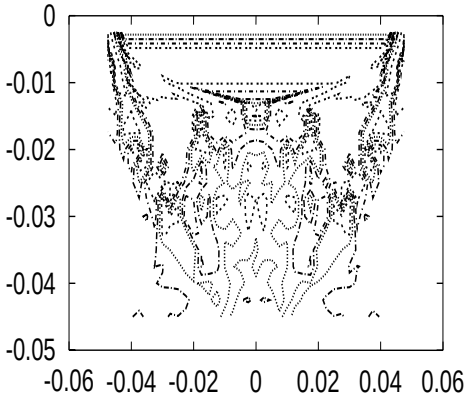

(d) Vertical (RANS+RFG)

Figure 15: Unsteady inlet velocity components: inlet conditions for LES of a ship-wake.

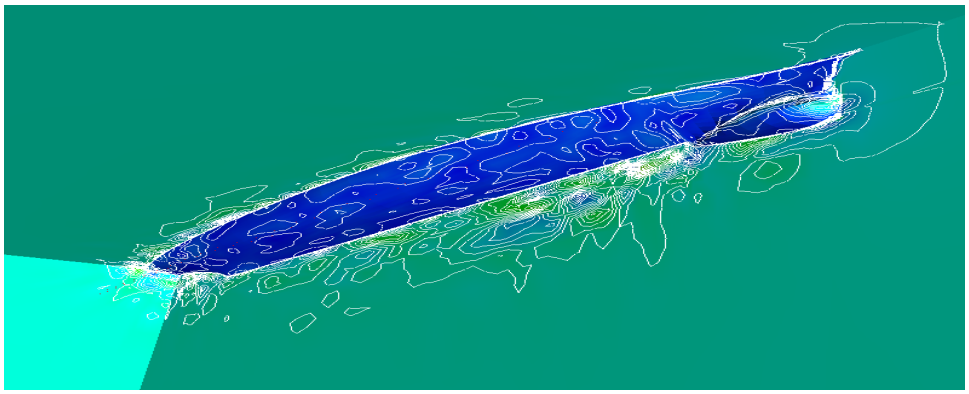

Figure 16: Turbulent velocity around a ship hull computed with the RFG algorithm.
View from below.

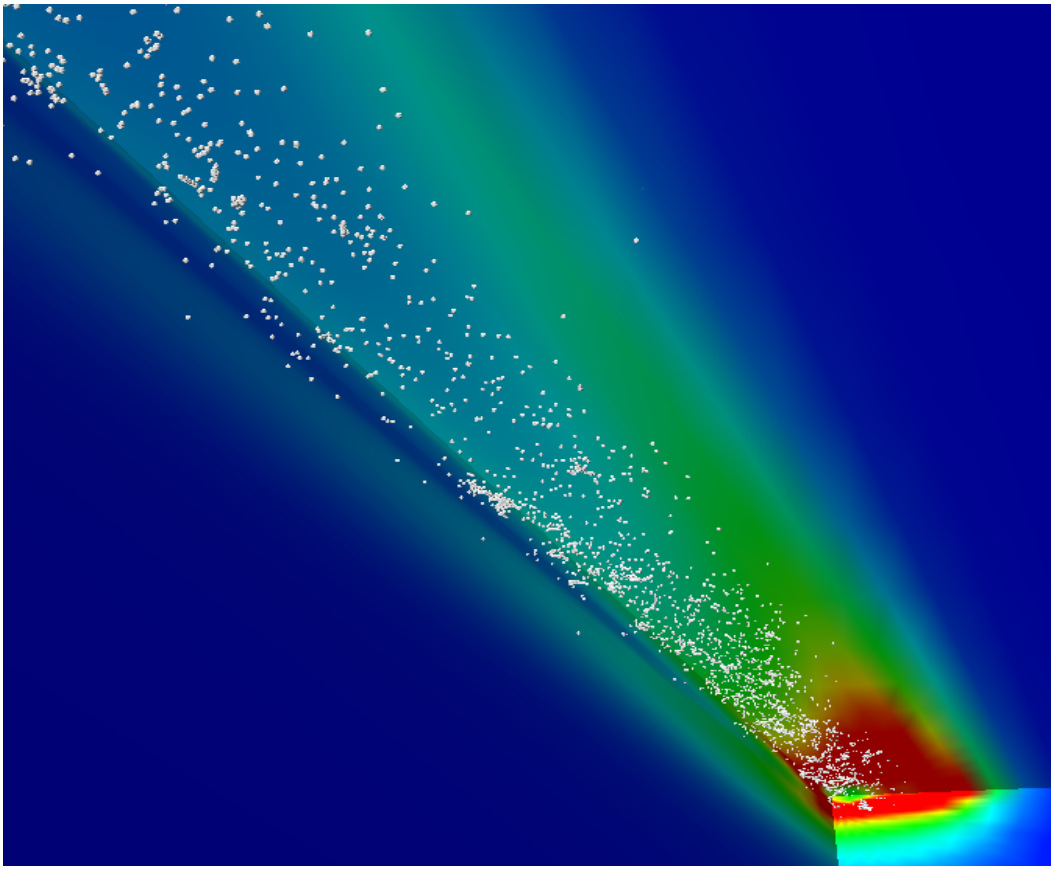

Figure 17: Bubbles in a ship-wake.
Background shading is according to the turbulent kinetic energy.

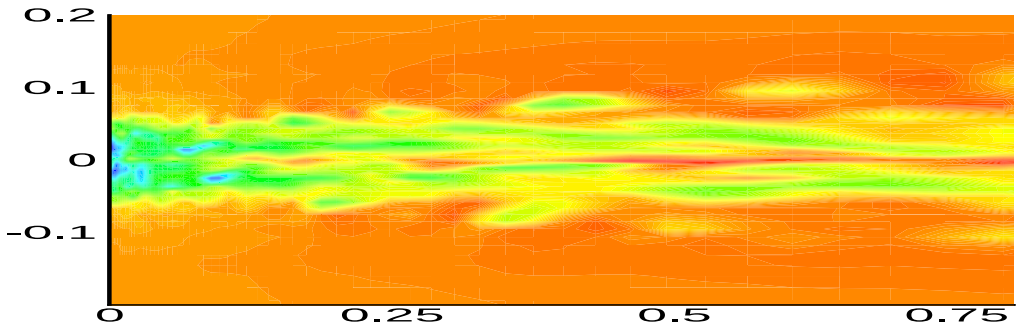

(a) Stream-wise velocity contours of the simulated wake flow

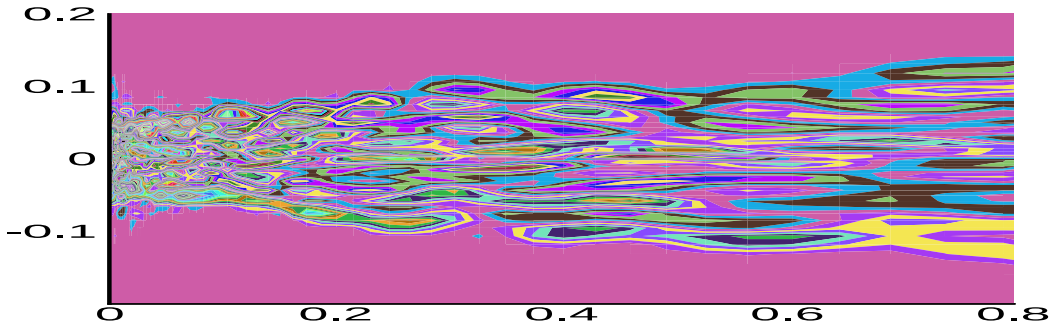

(b) Instantaneous vertical vorticity contours

Figure 18: LES of a ship-wake flow